https://doi.org/10.1016/j.jallcom.2017.09.052

Magnetoelastic and magnetocaloric properties of $Tb_{62.5}Co_{37.5}$ amorphous alloy

B. Z. Tang[1, 2], D.Q. Guo[2], L. Xia[1, *], D. Ding[1] and K. C. Chan[2, *]

[1] Laboratory for Microstructure, Institute of Materials, Shanghai University, Shanghai 200072, China &

[2] Department of Industrial and Systems Engineering, The Hong Kong Polytechnic University, Hung Hom, Hong Kong

Abstract

In the present work, we report the outstanding magneto-elastic and magneto-caloric properties of a Tb-Co binary amorphous alloy. The glass forming ability (GFA) of Tb-Co binary alloys was studied and the best glass former was obtained near the eutectic point of the binary alloys. The magnetic properties of the eutectic $Tb_{62.5}Co_{37.5}$ amorphous alloy were measured, and it was found that the $Tb_{62.5}Co_{37.5}$ amorphous ribbons exhibited excellent magneto-elastic properties (the magnetostriction of nearly 470 ppm at 50 K under 5 T) and magneto-caloric properties (the peak magnetic entropy change of 9.3 $Jkg^{-1}K^{-1}$ at 92.5 K under 5 T). The mechanism for the improved GFA, magneto-caloric effect (MCE) and magneto-elastic properties of the $Tb_{62.5}Co_{37.5}$ amorphous ribbons was analyzed.

Keywords: amorphous materials, rapid-solidification, magnetocaloric, magnetostriction, magnetic measurements, thermal analysis

* Corresponding authors. Email: xialei@shu.edu.cn (L. Xia) and kc.chan@polyu.edu.hk (K. C. Chan)

1. Introduction

Amorphous alloys with long-range disordered but short-range ordered structure, far from the equilibrium state and usually obtained by rapid quenching, have attracted both scientific and industrial interest because of their unique properties that are superior to their crystalline counterparts [1-2]. In general, amorphous alloys can be classified into two types: the structural and the functional amorphous alloys. Structural amorphous alloys usually require outstanding glass forming ability (GFA) so as to obtain bulk amorphous samples, with high strength and large plasticity, etc [1-9]. Functional amorphous alloys are primarily concerned with outstanding or even extraordinary physical and chemical properties, such as better magnetic properties, super-hydrophobic and catalyzing characteristics, good corrosion resistance, and so on [1-2, 10-15].

Among the functional amorphous alloys, more and more attention has been paid to the rare-earth (RE)-transition metal (TM)-based amorphous alloys because of their excellent magnetic properties. For example, Gd-TM-based amorphous alloys show an excellent magneto-caloric effect (MCE) [14-21]; Nd-TM-based bulk metallic glasses exhibit anomalous hard magnetic properties [22-25]; amorphous (Tb, Dy)-TM-based films show the extraordinary magneto-elastic properties [26-27].

It is usually considered that the magnetostriction of an amorphous alloy is small when compared to that of its single-crystal or sintered alloy counter-part because the randomness in the microstructures of the amorphous materials suppresses the magneto-elastic interactions [28-31]. For example, $Fe_{43}Co_{27}B_{19}Si_5Nb_4C_2$ metallic glass only demonstrates a magnetostriction of 38 ppm under a magnetic field of 3 kOe, whereas (Fe-Co)-B-Si-Nb metallic glasses only achieve magnetostriction in the range of 9 ~ 12 ppm. However, TbDyFe amorphous thin films show much larger magnetostriction. $(Tb_{0.3}Dy_{0.7})_{40}Fe_{60}$ amorphous films showed magneto-striction up to 300 ppm under a magnetic field of 1000 Oe field when the substrate temperature was in the range from 603 K to 670 K [26]. Recently, Speliotis *et al.* have further reported that an amorphous TbDyFe thin films demonstrated a magnetostriction up to 400 ppm under a magnetic

field of 1 kOe [27]. Although amorphous TbDyFe thin films have demonstrated very good magnetostriction, the GFA of these amorphous films is not high enough, and the mechanisms for the high magnetostriction of these RE-TM amorphous alloys have not been deeply investigated. In the present work, we studied the GFA of a simple binary Tb-Co amorphous alloy system, and identified the best glass former in this binary alloy system for investigating its magnetocaloric and magnetoelastic properties. The findings will shed more light on the mechanisms for high magnetostriction of multicomponent amorphous alloys.

2. Experimental procedure

Ingots of binary Tb-Co alloys with nominal compositions Tb_xCo_{100-x} (x=35, 40, 45, 50, 55, 60, 62.5, 64, 65, 70 and 80) were prepared by arc-melting a mixture of the Tb and Co elements with purity of at least 99.9% (at%). As-spun ribbons were produced by melt-spinning in a high-purified argon atmosphere using a single copper wheel with a speed of 30 m/s. The compositions of the as-spun ribbons are ascertained by an Oxford INCA energy dispersive spectrometer (EDS) on a JEOL JSM-6700F scanning electron microscope (SEM). The structure of the ribbons was characterized by X-ray diffraction (XRD) on a Rigaku D\max-2550 diffractometer using Cu K_α radiation and a JEOL JEM-2010F high resolution electron microscope (HREM). For HREM observations, specimens were prepared by ion-polishing under a pure argon atmosphere using the GATAN 691 precision ion-polishing system. The thermal properties of the amorphous ribbons were measured by Perkin-Elmer DIAMOND differential scanning calorimetry (DSC) under a purified argon atmosphere at a heating rate of 20 K/min. A Quantum Design Physical Properties Measurement System (PPMS 6000) was used to measure the magnetic properties of the amorphous ribbons. As spun ribbons, with approximate dimensions of 8 mm (long)×0.6 mm (wide)×40 μm (thick), were glued together for magnetic measurements. The applied field is parallel to the longitudinal direction along the length of the sample so as to minimize the demagnetization factor. The temperature dependence of the magnetization (*M*-*T*) curve was measured under a field of 0.03 T in

the cooling process. The hysteresis loops were measured at 75 K and 150 K under a field of 5 T. The isothermal magnetization curves (*M*-*H*) of the amorphous ribbons were measured at selected temperatures under a field of 5 T. The magnetostriction (λ) of the $Tb_{62.5}Co_{37.5}$ amorphous ribbon was measured by PPMS at 50 K, 60 K, 70 K, 80 K and 90 K using a foil strain gauge (KYOWA; model KFL-02-120-C1) under a magnetic field of 5 T, which was placed perpendicular to the longitudinal direction along the length of the sample. The gauge, which was calibrated by pure aluminum, was fixed on the $Tb_{62.5}Co_{37.5}$ amorphous sample with KYOWA PC-600 strain gauge cement.

3. Results and discussion

Figure 1 shows the XRD patterns of the Tb_xCo_{100-x} (x=35, 40, 45, 50, 55, 60, 62.5, 64, 65, 70 and 80) as-spun ribbons. $Tb_{45}Co_{55}$, $Tb_{50}Co_{50}$, $Tb_{55}Co_{45}$, $Tb_{60}Co_{40}$ and $Tb_{62.5}Co_{37.5}$ ribbons exhibit typical amorphous characteristics of broadened diffraction maxima in the XRD patterns, while $Tb_{35}Co_{65}$, $Tb_{40}Co_{60}$, $Tb_{64}Co_{36}$, $Tb_{65}Co_{35}$, $Tb_{70}Co_{30}$ and $Tb_{80}Co_{20}$ are partially or fully crystallized.

3.1 Glass forming ability of the alloys

The GFA of Tb-Co binary alloys can be studied in more detail using the DSC measurement of the amorphous ribbons. Figure 2 shows the continuous DSC traces of the Tb_xCo_{100-x} (x=45, 50, 55, 60, 62.5) amorphous ribbons obtained at a heating rate of 20 K/min. The endothermic glass transition behavior before crystallization in the DSC traces of these as-spun ribbons also illustrates their amorphous characteristics. The onset temperatures for the glass transition (T_g) and the crystallization (T_x) for each amorphous ribbon, as listed in TABLE I, are shown on the continuous DSC traces. The liquidus temperatures (T_l) of the amorphous ribbons obtained from the equilibrium phase diagram are also listed in Table I. Therefore, we can obtain the reduced glass transition temperature (T_{rg}) and the parameter γ ($=T_x/(T_g+T_l)$) of the Tb_xCo_{100-x} (x=45, 50, 55, 60, 61, 62.5) amorphous alloys, both of which are the mostly used parameter for evaluating the GFA of the alloys [3, 9]. Figure 3 (a) shows the compositional dependence of T_{rg} and γ of the Tb_xCo_{100-x} (x=45, 50, 55, 60, 61, 62.5) amorphous

ribbons. Both T_{rg} and γ increase with the increase of Tb content, indicating that the eutectic $Tb_{62.5}Co_{37.5}$ amorphous alloy is the best glass former among the Tb-Co binary alloys, which agrees with one of the glass forming criteria, i. e., the deep eutectic rule [9, 32]. The amorphous structure of the $Tb_{62.5}Co_{37.5}$ amorphous alloy was ascertained by the HREM images of the as-spun ribbon, as shown in Fig. 3 (b). The $Tb_{62.5}Co_{37.5}$ amorphous ribbon is fully amorphous with only short ranged orders, and no obvious crystalline phases have been found in the amorphous matrix.

3.2 Magnetic properties of the amorphous alloys

Figure 4 (a) shows hysteresis loops of the $Tb_{62.5}Co_{37.5}$ amorphous ribbon measured at 75 K and 150 K. The amorphous ribbon is paramagnetic at 150 K and is soft magnetic at 75 K, with a negligible coercivity. The *M-T* curves of the $Tb_{62.5}Co_{37.5}$ amorphous ribbon and its crystalline analogue obtained under a field of 0.03 T are shown in Fig. 4 (b). The Curie temperature (T_c) of the $Tb_{62.5}Co_{37.5}$ amorphous and crystalline ribbons obtained from the derivative of the *M-T* curves are about 92 K and 104 K, as marked on the *M-T* curves respectively. The effective magnetic moment (μ_{eff}) of the $Tb_{62.5}Co_{37.5}$ amorphous and crystalline ribbons were obtained from the plots of the ratio *H*/*M* as a function of temperature according to the Curie–Weiss law, as shown in the inset of Fig. 4 (b). Here μ_{eff} is about 8.20 μ_B for amorphous ribbons, and is about 6.46 μ_B for crystalline ribbons. It is worth noting that the crystalline $Tb_{62.5}Co_{37.5}$ alloy is composed of two phases: 88.5% (at%) Tb_4Co_3 phase and 11.5 % (at%) $Tb_{12}Co_7$ phase. However, the derivative of the *M-T* curve shows that there is only one magnetic phase in the crystalline $Tb_{62.5}Co_{37.5}$ alloy, indicating that one of crystalline phases is paramagnetic. Thus, the magnetic properties of the crystalline ribbon, including the saturation magnetization, Curie temperature and magnetic entropy change of the $Tb_{62.5}Co_{37.5}$ crystalline alloy, are supposed to be mainly contributed by the Tb_4Co_3 phase because μ_{eff} of the crystalline ribbon is close to the nominal magnetic moment (μ_{nom}) of 88.5% (at%) Tb_4Co_3 phase.

Derived from the *M-H* curves of the amorphous ribbons measured at different temperatures, we can obtain the temperature dependence of the magnetic entropy

change ((-ΔS_m)-T) curves according to the thermodynamic Maxwell equation. Figure 5 (a) shows the (-ΔS_m)-T curves of the $Tb_{62.5}Co_{37.5}$ amorphous ribbon under various magnetic fields. The $Tb_{62.5}Co_{37.5}$ amorphous ribbons exhibit rather high -ΔS_m^{peak} values compared with other amorphous alloys [14-21]: 2.8 $Jkg^{-1}K^{-1}$ under 1 T, 3.9 $Jkg^{-1}K^{-1}$ under 1.5 T, 4.8 $Jkg^{-1}K^{-1}$ under 2 T, 5.7 $Jkg^{-1}K^{-1}$ under 2.5 T, 6.5 $Jkg^{-1}K^{-1}$ under 3 T, 7.3 $Jkg^{-1}K^{-1}$ under 3.5 T, 8.0 $Jkg^{-1}K^{-1}$ under 4 T, 8.6 $Jkg^{-1}K^{-1}$ under 4.5 T and 9.3 $Jkg^{-1}K^{-1}$ under 5 T at 92.5 K, respectively. For comparison purpose, we also obtain the (-ΔS_m)-T curves of the $Tb_{45}Co_{55}$ amorphous ribbon. Figure 5 (b) shows the (-ΔS_m)-T curves of the $Tb_{62.5}Co_{37.5}$ and $Tb_{45}Co_{55}$ amorphous ribbons under the fields of 1.5 T and 5 T. The -ΔS_m^{peak} values of the $Tb_{62.5}Co_{37.5}$ amorphous alloy are much higher than those of the $Tb_{45}Co_{55}$ amorphous ribbon, which is most likely related to the higher magnetic moment of $Tb_{62.5}Co_{37.5}$ amorphous alloy due to its high Tb concentration and the high magnetic moment of the Tb^{3+} ions (~9.72 μ_B).

From the (-ΔS_m)-T curves obtained under various magnetic fields, we can also construct the -ΔS_m-H relationship, which is useful for better understanding the physical characteristics of the magneto-caloric behavior of the $Tb_{62.5}Co_{37.5}$ amorphous alloy [17, 33, 34]. As is known, the field dependence of -ΔS_m follows a linear relationship with H^n ($-\Delta S_m \propto H^n$) except in a very weak magnetic field or a very strong magnetic field. The n value can be therefore obtained by $n = \frac{d \ln|\Delta S_m|}{d \ln H}$. For ferromagnets, $n \approx 2$ at the temperature well above T_c according to Curie-Weiss law, and depends on the magnetic state of the materials at the temperature below or near T_c. For materials with unignorable hysteresis, the effect of hysteresis on -ΔS_m and the -ΔS_m-H relationship has to be considered and no analytical expression is available. For soft magnetic amorphous materials, n is close to 1 at a temperature well below T_c and decrease to 0.72~0.75 near T_c [33-36]. The temperature dependence of n (n-T) curve of the $Tb_{62.5}Co_{37.5}$ amorphous alloy, as shown in the inset of Fig. 5 (b), illustrates the typical magneto-caloric behavior of a soft magnetic amorphous material with a second-order magnetic phase transition. On the other hand, n=0.746 near T_c, which is larger than the one proposed from the mean field theory but is more in agreement with the result predicted by the Arrott-

Noakes equation [34-35], also ascertains its typical amorphous structure of numerous short range order embedded in the disordered matrix, because bulk amorphous samples with more complicated microstructures will exhibit a larger n value near T_c [14].

Figure 6 shows the field dependence of the reversible magnetostriction (λ-H) curves of the $Tb_{62.5}Co_{37.5}$ amorphous ribbon measured at 50 K, 60 K, 70 K, 80 K and 90 K under a field of 5 T. Similar to some TbDyFe amorphous thin films [26-27], the $Tb_{62.5}Co_{37.5}$ amorphous ribbon shows rather high magnetostriction up to 320 ppm under a field of 2 T, and nearly 470 ppm under a field of 5 T at 50 K. The large magnetostriction in Tb(Dy)-TM amorphous alloys is anomalous according to the random anisotropy model for magnetostriction developed by O'Handley and Grant [30-31]. In this model, the amorphous alloys are zero-magnetostriction alloys because the clusters are considered to be identical grains without any interaction between each other. However, the randomly oriented clusters surrounded by the disordered matrix in amorphous alloys are not identical in either the microstructure or the size and shape. Furthermore, the interaction between the clusters and the disordered matrix cannot be omitted. The clusters will rotate in order to minimize their local anisotropic energy upon magnetization. The rigid rotation will give rise to shear stresses on the surrounded matrix, which will result in macro-deformation of the whole specimen and lead to the high magnetostriction of the Tb(Dy)-TM amorphous alloys. The binary $Tb_{62.5}Co_{37.5}$ amorphous alloy with a combination of good GFA and excellent magnetostriction provides a simple foundation for our future work on the modeling of the mechanism for the large magnetostriction in Tb(Dy)-TM amorphous alloys. On the other hand, although the $Tb_{62.5}Co_{37.5}$ amorphous alloy shows large magnetostriction, it cannot be applied in magnetoelastic sensors because of its low Curie temperature. However, considering the simple composition of the binary alloys, the GFA, T_c and magnetic properties of the amorphous alloys can easily be tuned by compositional adjustment. Therefore, the binary $Tb_{62.5}Co_{37.5}$ amorphous alloy with larger magnetostriction will play an important role for developing multicomponent amorphous alloys with enhanced GFA and magnetoelastic properties at the temperature higher than 50 K or even near

room temperature.

4. Conclusions

In summary, we studied the GFA of Tb-Co binary alloys and obtained the eutectic $Tb_{62.5}Co_{37.5}$ amorphous alloy as the best glass former in the binary alloy system. HREM observation has ascertained the fully amorphous microstructure of the as-spun $Tb_{62.5}Co_{37.5}$ ribbon. The magnetic measurements of the $Tb_{62.5}Co_{37.5}$ binary amorphous alloy show the excellent magneto-caloric and magneto-elastic properties of the $Tb_{62.5}Co_{37.5}$ amorphous alloy. The $-\Delta S_m^{peak}$ of the $Tb_{62.5}Co_{37.5}$ amorphous alloy is rather high compared with other amorphous alloys. The $-\Delta S_m$-H relationship of the $Tb_{62.5}Co_{37.5}$ amorphous alloy illustrates the typical magnetocaloric behavior of fully amorphous alloys. The magnetoelastic properties of the $Tb_{62.5}Co_{37.5}$ amorphous alloys were measured below the Curie temperatures and a rather high magnetostriction (up to 320 ppm under a field of 2 T and nearly 470 ppm under a field of 5 T) was obtained at 50 K. The binary $Tb_{62.5}Co_{37.5}$ amorphous alloy with a combination of good GFA and excellent magnetostriction not only provides a simple model for investigating the mechanism of large magnetostriction in Tb(Dy)-TM amorphous alloys, but also shows a promising perspective in industrial applications as a basic alloy for developing multicomponent amorphous alloys with improved GFA and magnetoelastic properties.

Acknowledgements

The work described in this paper was supported by the Hong Kong Polytechnic University (grant number G-YBJG), and the National Nature Science Foundation of China (grant numbers 51271103, 51671119).

References

[1] M. Miller and P. Liaw, Bulk Metallic Glasses, Springer, 2008.

[2] C. Suryanarayana and A. Inoue, Bulk metallic glasses, CRC Press, 2011.

[3] D. Turnbull, Under what conditions can a glass be formed?, Contemp. Phys. 10 (1969) 473-488.

[4] W. L. Johnson, Bulk Glass-Forming Metallic Alloys: Science and Technology, MRS Bull., 24 (1999) 42-56.

[5] A. L. Greer, Metallic glasses…on the threshold, Mater. Today, 12 (2009) 14-22.

[6] W. H. Wang, The elastic properties, elastic models and elastic perspectives of metallic glasses, Prog. Mater. Sci., 57 (2012) 487-656.

[7] M. M. Trexler, N.N. Thadhani, Mechanical properties of bulk metallic glasses, Prog. Mater. Sci., 55 (2010) 759-839.

[8] J. Schroers, Processing of Bulk Metallic Glass, Adv. Mater., 22 (2010) 1566-1597.

[9] Z. P. Lu, C. T. Liu, Glass Formation Criterion for Various Glass-Forming Systems, Phys. Rev. Lett. 91 (2003) 115505.

[10] T. Bitoh, A. Makino and A. Inoue, Magnetization Process and Coercivity of Fe-(Al, Ga)-(P, C, B, Si) Soft Magnetic Glassy Alloys, Mater. Trans. 45 (2004) 1219-1227.

[11] M. Naka, K. Hashimoto and T. Masumoto, High Corrosion Resistance of Chromium-Bearing Amorphous Iron Alloys in Neutral and Acidic Solutions Containing Chloride, Corrosion, 32 (1976) 146-152.

[12] Y. C. Hu, Y. Z. Wang, R. Su, C. R. Cao, F. Li, C. W. Sun, Y. Yang, P. F. Guan, D. W. Ding, Z. L. Wang and W. H. Wang, A Highly Efficient and Self-Stabilizing Metallic-Glass Catalyst for Electrochemical Hydrogen, Adv. Mater. 28 (2016) 10293-10297

[13] J. Ma, X. Y. Zhang, D. P. Wang, D. Q. Zhao, D. W. Ding, K. Liu and W. H. Wang, Superhydrophobic metallic glass surface with superior mechanical stability and corrosion resistance, Appl. Phys. Lett. 104 (2014) 173701.

[14] L. Xia, Q. Guan, D. Ding, M. B. Tang and Y. D. Dong, Magneto-caloric response of the $Gd_{60}Co_{25}Al_{15}$ metallic glasses, Appl. Phys. Lett. 105 (2014) 192402.

[15] Q. Luo, D.Q. Zhao, M.X. Pan, W.H. Wang, Magnetocaloric effect in Gd-based bulk metallic glasses, Appl. Phys. Lett. 89 (2006) 081914.

[16] J. Du, Q. Zheng, Y. B. Li, Q. Zhang, D. Li and Z. D. Zhang, Large magnetocaloric effect and enhanced magnetic refrigeration in ternary Gd-based bulk metallic glasses, J. Appl. Phys. 103 (2008) 023918.

[17] L. Xia, K. C, Chan, M. B. Tang and Y. D. Dong, Large magnetic entropy change and adiabatic temperature rise of a $Gd_{55}Al_{20}Co_{20}Ni_5$ bulk metallic glass, J. Appl. Phys. 115 (2014) 223904.

[18] F. Yuan, J. Du and B. Shen, Controllable spin-glass behavior and large magnetocaloric effect in Gd-Ni-Al bulk metallic glasses, Appl. Phys. Lett. 101 (2012) 032405.

[19] Z. W. Wang, P. Yu, Y. T. Cui and L. Xia, Near room temperature magneto-caloric effect of a $Gd_{48}Co_{52}$ amorphous alloy, J. Alloys Compd. 658 (2016) 598-602.

[20] X. C. Zhong, P. F. Tang, Z. W. Liu, D. C. Zeng, Z. G. Zheng, H. Y. Yu, W. Q. Qiu and M. Zou, Magnetic properties and large magnetocaloric effect in Gd–Ni amorphous ribbons for magnetic refrigeration applications in intermediate temperature range, J. Alloys Compd. 509 (2011) 6889-6892.

[21] G. L. Liu, D. Q. Zhao, H. Y. Bai, W. H. Wang and M. X. Pan, Room temperature table-like magnetocaloric effect in amorphous $Gd_{50}Co_{45}Fe_5$ ribbon, J. Phys. D: Appl. Phys. 49 (2016) 055004.

[22] A. Inoue, T. Zhang, W. Zhang and A. Takeuchi, Bulk Nd-Fe-Al Amorphous Alloys with Hard Magnetic Properties, Mater. Trans. JIM, 37 (1996) 99-108.

[23] S. Schneider, A. Bracchi, K. Samwer, M. Seibt and P. Thiyagarajan, Microstructure-controlled magnetic properties of the bulk glass-forming alloy $Nd_{60}Fe_{30}Al_{10}$, Appl. Phys. Lett. 80 (2002) 1749.

[24] B. C. Wei, W. Löser, L. Xia, S. Roth, M. X. Pan, W. H. Wang, Anomalous thermal stability of Nd–Fe–Co–Al bulk metallic glass, Acta Mater. 50 (2002) 4357-4367.

[25] L. Xia, S. S. Fang, C. L. Jo and Y. D. Dong, Glass forming ability and microstructure of hard magnetic $Nd_{60}Al_{20}Fe_{20}$ glass forming alloy, Intermetallics,

14 (2006) 10981101.

[26] A. Speliotis and D. Niarchos, Magnetostrictive properties of amorphous and crystalline TbDyFe thin films, Sens. Actuators A, 106 (2003) 298.

[27] Th. Speliotis and D. Niarchos, Extraordinary magnetization of amorphous TbDyFe films, Microelectro. Eng., 112 (2013) 183.

[28] A. Inoue, B. L. Shen and C. Chang, Superhigh strength of over 4000 MPa for Fe-based bulk glassy alloys in $[(Fe_{1-x}Co_x)_{0.75}B_{0.2}Si_{0.05}]_{96}Nb_4$ system, Acta Mater., 52 (2004) 4093.

[29] D. Atkinson, P. T. Squire, M. R. J. Gibbs and S. N. Hogsdon, Implications of magnetic and magnetoelastic measurements for the domain structure of FeSiB amorphous wires, J. Phys. D: Appl. Phys. 27 (1994) 1354.

[30] R. C. O'Handley and R. J. Grant, in: Proc. Conf. on Rapidly Quenched Metals, edited by S. Steeb and H. Warlimont, (Elsevier, Amsterdam, 1985), p. 1125.

[31] J. M. Barandiarán, J. Gutiérrez and A. Garcia-Arribas, Magneto-elasticity in amorphous ferromagnets: Basic principles and applications, Phys. Status Solidi A, 208 (2011) 2258-2264.

[32] A. Inoue, Stabilization of metallic supercooled liquid and bulk amorphous alloys, Acta Mater. 48 (2000) 279-306.

[33] V. Franco, J. S. Blázquez, and A. Conde, The influence of Co addition on the magnetocaloric effect of Nanoperm-type amorphous alloys, J. Appl. Phys. 100 (2006) 064307.

[34] V. Franco, J. M. Borrego, C. F. Conde, A. Conde, M. Stoica, and S. Roth, Refrigerant capacity of FeCrMoCuGaPCB amorphous alloys, J. Appl. Phys. 100 (2006) 083903.

[35] H. Oesterreicher and F. T. Parker, Magnetic cooling near Curie temperatures above 300 K, J. Appl. Phys. 55 (1984) 4334.

[36] V. Basso, G. Bertotti, M. LoBue and C.P. Sasso, Theoretical approach to the magnetocaloric effect with hysteresis, J. Magn. Magn. Mater. 290-291 (2005) 654.

Figure captions

Figure 1 XRD patterns of the Tb_xCo_{100-x} (x=35, 40, 45, 50, 55, 60, 62.5, 64, 65, 70, 80) as-spun ribbons obtained at the wheel surface speed of 30 m/s.

Figure 2 DSC traces of the Tb_xCo_{100-x} (x=45, 50, 55, 60, 62.5) amorphous ribbons obtained at a heating rate of 20 K/min.

Figure 3 (a) The compositional dependence of T_{rg} and γ of the Tb_xCo_{100-x} (x=45, 50, 55, 60, 62.5) amorphous ribbons; (b) the HREM image of the $Tb_{62.5}Co_{37.5}$ as-spun ribbon.

Figure 4 (a) The hysteresis loops of the $Tb_{62.5}Co_{37.5}$ amorphous ribbon measured at 75 K and 150 K; (b) The *M*-*T* curves of the $Tb_{62.5}Co_{37.5}$ amorphous ribbon and its crystalline analogue obtained under a field of 0.03 T; the inset is the plots of the ratio *H*/*M* as a function of temperature for the $Tb_{62.5}Co_{37.5}$ amorphous and crystalline ribbons.

Figure 5 (a) $(-\Delta S_m)$-*T* curves of the $Tb_{62.5}Co_{37.5}$ amorphous ribbon under various magnetic fields, the inset is the *n*-*T* curve of the $Tb_{62.5}Co_{37.5}$ amorphous alloy; (b) $(-\Delta S_m)$-*T* curves of the $Tb_{62.5}Co_{37.5}$ and $Tb_{45}Co_{55}$ amorphous ribbons under the fields of 1.5 T and 5 T.

Figure 6 The magnetostriction curves of the $Tb_{62.5}Co_{37.5}$ amorphous ribbon measured at 50 K, 60 K, 70 K, 80 K and 90 K under a field of 5 T.

TABLE I The onset temperatures of glass transition (T_g^{onset}), the crystallization (T_x^{onset}), the liquidus temperature (T_l), the reduced glass transition temperature (T_{rg}) and the parameter γ of Tb_xCo_{100-x} amorphous ribbons

Tb_xCo_{100-x} ribbons	T_g^{onset} (K)	T_x^{onset} (K)	T_l (K)	T_{rg}	γ
x=45	508	578	1360	0.374	0.309
x=50	535	587	1290	0.415	0.322
x=55	527	592	1190	0.443	0.345
x=60	537	592	1053	0.51	0.372
x=62.5	536	587	968	0.554	0.390

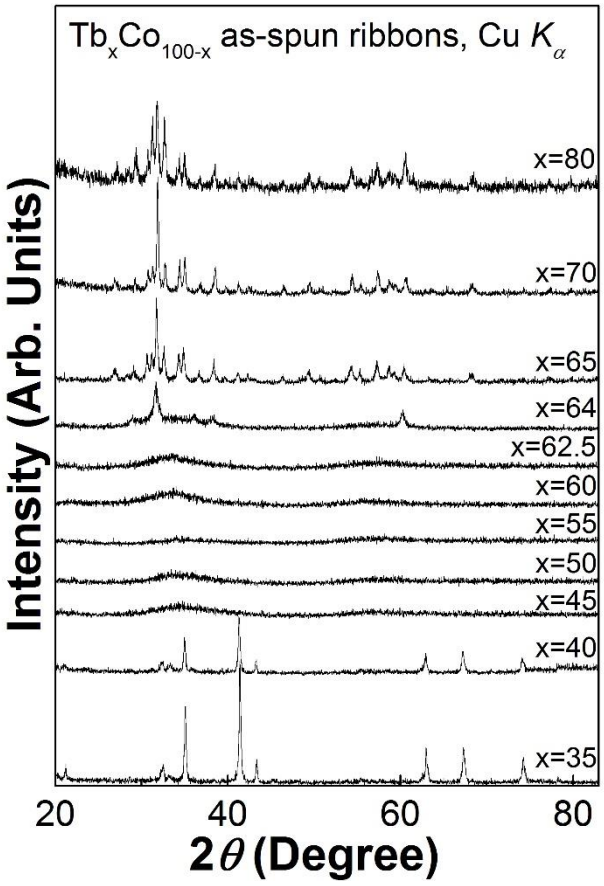

B. Z. Tang *et. al*

Figure 1

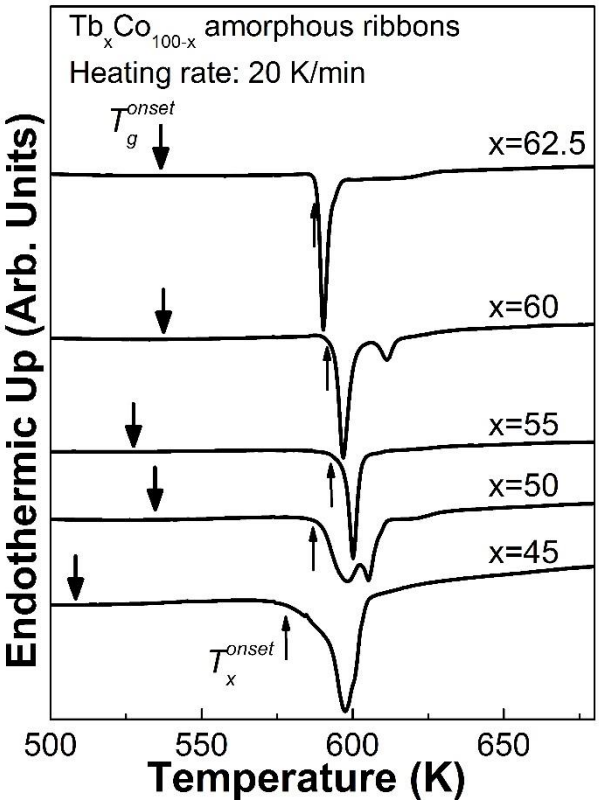

B. Z. Tang *et. al*

Figure 2

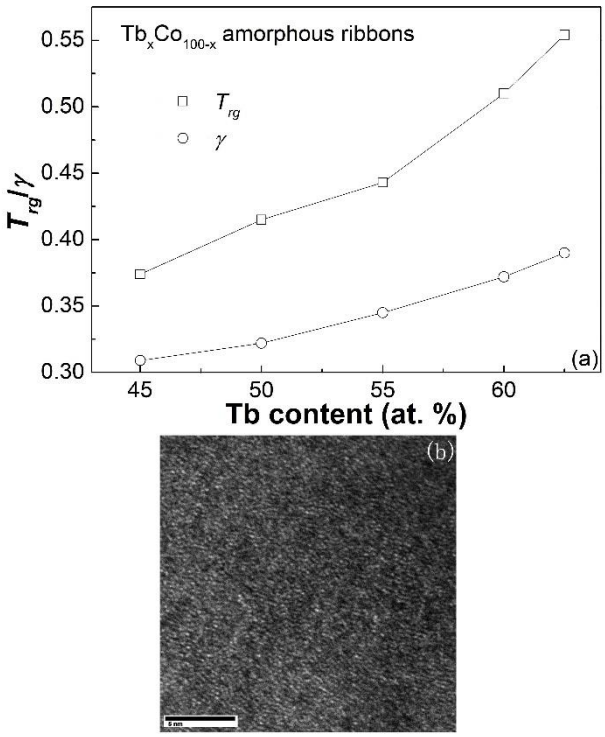

B. Z. Tang *et. al*

Figure 3

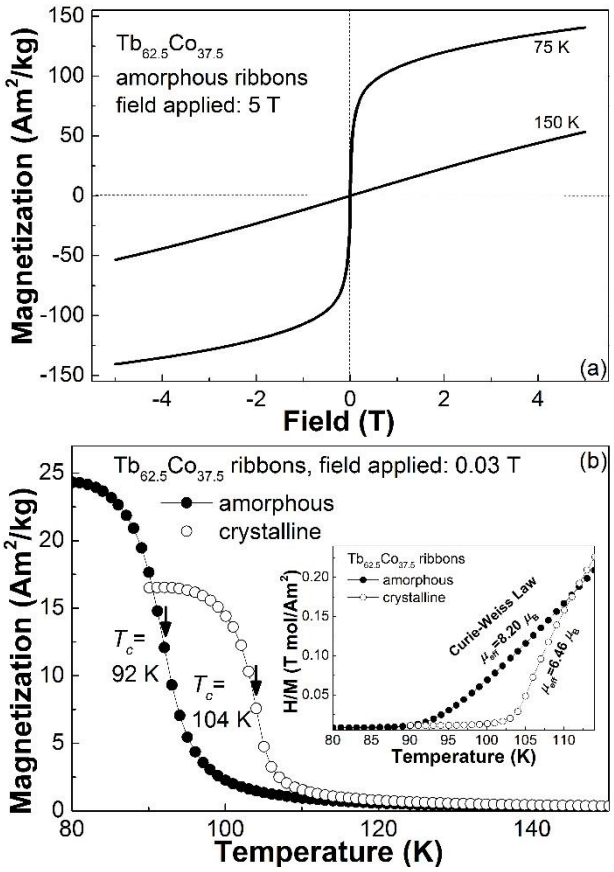

B. Z. Tang *et. al*

Figure 4

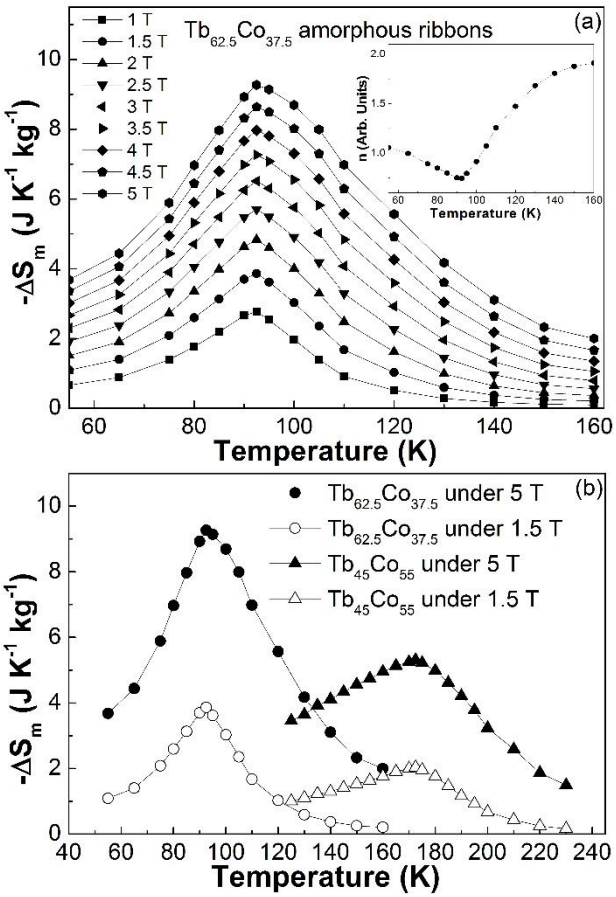

B. Z. Tang *et. al*

Figure 5

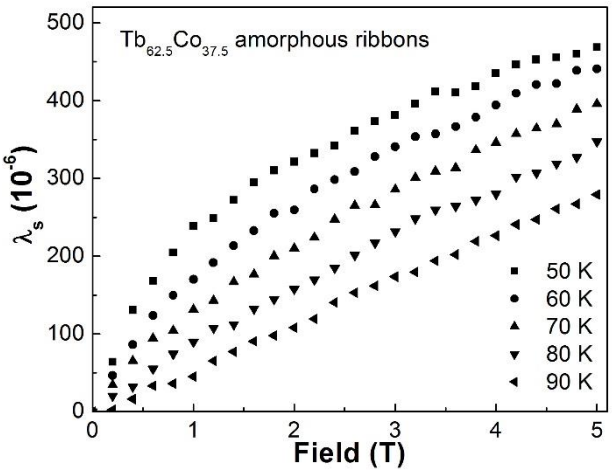

B. Z. Tang *et. al*

Figure 6